INTERNATIONAL JOURNAL FOR NUMERICAL METHODS IN FLUIDS
Int. J. Numer. Meth. Fluids 2004; **46**:163–182 (DOI: 10.1002/fld.751)

A γ-model BGK scheme for compressible multifluids

Song Jiang*,† and Guoxi Ni‡

LCP, Institute of Applied Physics and Computational Mathematics, P.O. Box 8009, Beijing 100088, China

SUMMARY

We present a γ-model BGK scheme for the numerical simulation of compressible multifluids. The scheme is based on the incorporation of a conservative γ-model scheme given in (*J. Comput. Phys.* 1996; **125**:150–160) into the gas kinetic BGK scheme (*J. Comput. Phys.* 1993; **109**:53–66, *J. Comput. Phys.* 1994; **114**:9–17), and is simple to implement. Several numerical examples presented in this paper validate the scheme in the application of compressible multimaterial flows. Copyright © 2004 John Wiley & Sons, Ltd.

KEY WORDS: γ-model BGK scheme; compressible multifluids; γ-model; gas kinetic BGK scheme; directional splitting

1. INTRODUCTION

In this paper we present a γ-model BGK scheme for compressible multifluids by incorporating a γ-model scheme [1] and the gas kinetic BGK scheme given in References [2–4].

In the past years the development of gas kinetic schemes for the simulation of compressible fluids has attracted much attention and significant progress has been made. In the gas kinetic theory, the Euler and compressible Navier–Stokes equations can be derived from the Boltzmann equation using the zero and first-order Chapman–Enskog expansion. The Euler and compressible Navier–Stokes equations can be theoretically obtained also by solving the simplified Bolztmann equation, i.e. the Bhatnagar–Gross–Krook model [5, 6]. In term of the gas kinetic representation, all flow variables are moments of a single particle distribution function. In the class of schemes called Boltzmann-type schemes (see e.g. References [7–18]), the free transport equation or the collisionless Boltzmann equation is solved in the gas evolution stage for the flux evaluation, then the collision part is implicitly implemented inside each cell. Based

*Correspondence to: S. Jiang, LCP, Institute of Applied Physics and Computational Mathematics, P.O. Box 8009, Beijing 100088, China.
†E-mail: jiang@mail.iapcm.ac.cn
‡E-mail: gxni@mail.iapcm.ac.cn

Contract/grant sponsor: Special Funds for Major State Basic Research Projects; contract/grant number: G1999032801
Contract/grant sponsor: NSFC; contract/grant number: 10225105
Contract/grant sponsor: CAEP

Published online 14 July 2004

Received 29 March 2003

on a collisional BGK model, Xu and Prendergast [2, 3] in 1993/1994 proposed a gas kinetic BGK scheme. The BGK scheme differs from the Boltzmann-type schemes mainly on the inclusion of particle collisions in the gas evolution stage. Instead of solving the collisionless Boltzmann equation, the BGK scheme uses a collisional BGK model in the numerical flux evaluation. Since the gas evolution process is a relaxation process from a non-equilibrium state to an equilibrium one, the entropy condition is always satisfied by the BGK scheme. Moreover, due to its specific governing equation, the BGK scheme gives the compressible Navier–Stokes equations in smooth regions, and provides a delicate dissipative mechanism, which is controlled by the pseudo-particle collision time and the intrinsic collisional model, to get a stable and crisp shock transition in non-smooth regions. After the introduction of the BGK scheme, there has been continuous and further development in this area, see References [19–23] on compressible multicomponent flows, References [24, 25] on magnetohydrodynamics, and References [26, 27] on the BGK scheme on unstructured meshes and a discontinuous Galerkin BGK method, and among others.

Over the past decades, significant progress has been made in the development of Eulerian numerical schemes for compressible multimaterial flows associated with discontinuities and shock waves, and a number of schemes have been proposed in the literature. Among them are methods, which use an extended conservative system of governing equations in which additional conservation equations are introduced to the original fluid equations to describe the conservation of parameters such as the level set functions, the mass fractions and the ratio of specific heats (γ-model) in the mixture, see e.g. References [1, 28–40] and among others. In order to maintain pressure equilibrium and the mass fraction positivity, and eliminate spurious oscillations and other computational inaccuracies near mass interfaces which are observed in these conservative methods References [1, 35, 40, 41], several non-conservative approaches to capture the contact discontinuities using an additional non-conservative governing equation are proposed [1, 41–48]. Recently, Xu and Lian [22, 23] presented a gas kinetic BGK scheme for multicomponent fluids. The basic idea in References [22, 23] is that time evolution of each component is governed by a BGK model with its own equilibrium state, and then, all the usual steps solving single component by the gas kinetic BGK method are used to each component, and the equilibrium states of both components are coupled in space and time due to the momentum and energy change in the course of particle collisions, and the common variables in the equilibrium states are the macroscopic velocity and temperature.

Our goal in this paper is to incorporate a developed multimaterial numerical method into the BGK scheme to propose a new gas kinetic BGK scheme for the simulation of compressible multifluids. In view of the framework of the BGK scheme and the process recovering the original equations by using local equilibrium states, for the multimaterial numerical methods mentioned above, the extended equations of conservation form, which govern the motion of interfaces, can (easily) be incorporated in the BGK scheme. Hence, in this paper we shall combine the BGK scheme with the γ-model in Reference [1] to present a so-called γ-model BGK scheme, where the interface of two materials with different specific heat ratios (γ) is considered to be a contact discontinuity of γ. Compared with Xu and Lian's scheme [22, 23] for which one needs to solve two BGK-models, the scheme of this paper is computationally cheaper, since only one BGK-model needs to be solved here. It should be pointed out here that the level set method can also be combined with the BGK scheme when the specific heat ratios of two materials are the same (cf. Reference [49]), while for different specific heat ratios, the level set method ([29], also cf. Reference [40]) cannot be easily incorporated in the

BGK scheme, because in this case it utilizes a transition function to transfer the two different specific heat ratios into the same one, and consequently, changes the constitutive equation of the pressure that cannot be easily recovered by using an appropriate local equilibrium state.

The paper is organized as follows. In Section 2, we derive the two space-dimensional γ-model BGK model for multifluids, and the one-dimensional model can be derived in the same manner. In Section 3, we give the algorithm formulation for the BGK model, and in Section 4 some numerical examples are presented to illustrate the availability and robustness of the scheme.

2. γ-BASED BGK MODEL

In this section, we derive the γ-based BGK model in two-space dimensions. In Reference [1] Abgrall introduced a γ-model non-conservative approach to capture contact discontinuities of two fluids using an additional non-conservative governing equation for the specific heat ratio γ in two-space dimensions,

$$\frac{\partial}{\partial t}\left(\frac{1}{\gamma-1}\right)+U\frac{\partial}{\partial x}\left(\frac{1}{\gamma-1}\right)+V\frac{\partial}{\partial y}\left(\frac{1}{\gamma-1}\right)=0 \tag{1}$$

where U and V are the macroscopic velocities in x and y directions, respectively. According to the analysis in Reference [1], this kind of Equation (1) can get correct pressure near the interface, while an earlier γ-model scheme [39, 40] uses γ instead of $1/(\gamma-1)$ and results in pressure non-equilibrium. Equation (1) can be easily written in the conservation form, using the conservation law of mass,

$$\frac{\partial}{\partial t}\left(\frac{\rho}{\gamma-1}\right)+\frac{\partial}{\partial x}\left(\frac{\rho U}{\gamma-1}\right)+\frac{\partial}{\partial y}\left(\frac{\rho V}{\gamma-1}\right)=0 \tag{2}$$

In the sequel, we add (2) to the Euler equations and discuss the corresponding BGK model from which the Euler equations coupled with (2) can be recovered. The BGK model in two-space dimensions can be written as (see e.g. Reference [4]),

$$f_t+uf_x+vf_y=\frac{g-f}{\tau} \tag{3}$$

where f is the gas distribution function and g is the equilibrium state approached by f, (u,v) is the particle velocity, both $f=f(x,y,t,u,v,z)$ and $g=g(x,y,t,u,v,z)$ are functions of x,y,t,u,v and the internal variable ξ,z, here the internal variable z is related to γ, the particle collision time τ is related to the viscosity and heat conduction coefficients. The equilibrium state is the Maxwellian distribution,

$$g=\rho\left(\frac{\lambda}{\pi}\right)^{(K+3)/2}\mathrm{e}^{-\lambda((u-U)^2+(v-V)^2+(z-Z)^2+\xi^2)}$$

where ρ is the macroscopic density, $Z=1/(\gamma-1)$ corresponds to (2), and $\lambda=m/2kT$ with m being the molecular mass, k the Boltzmann constant and T the macroscopic temperature. The total number of degree of freedom K in ξ is equal to $(5-3\gamma)/(\gamma-1)+1$, and ξ^2 denotes $\xi^2=\xi_1^2+\xi_2^2+\ldots+\xi_K^2$. The relation between the mass ρ, the momentum $\rho U,\rho V$, the energy

E and ρZ with the distribution function is

$$\begin{pmatrix} \rho \\ \rho U \\ \rho V \\ \rho Z \\ E \end{pmatrix} = \int \psi f \, \mathrm{d}\Xi \tag{4}$$

where

$$\psi = (\psi_1, \psi_2, \psi_3, \psi_4, \psi_5)^{\mathrm{T}} = \left(1, u, v, z, \tfrac{1}{2}(u^2 + v^2 + \xi^2)\right)^{\mathrm{T}}$$

and $\mathrm{d}\Xi = \mathrm{d}u\,\mathrm{d}v\,\mathrm{d}z\,\mathrm{d}\xi$ is the volume element in the phase space with $\mathrm{d}\xi = \mathrm{d}\xi_1 \ldots \mathrm{d}\xi_K$. Since the mass, the momentum and the energy are conservative during particle collisions, f and g satisfy the conservation constraint,

$$\int (g - f)\psi_\alpha \, \mathrm{d}\Xi = 0, \quad \alpha = 1, 2, 3, 4, 5 \tag{5}$$

at any point in space and time.

For a local equilibrium state with $f = g$, the Euler equations can be obtained by taking the moments of ψ to Equation (3), which leads to

$$\int \psi_\alpha (g_t + u g_x + v g_y) \, \mathrm{d}\Xi = 0$$

and the corresponding Euler equations coupled with (2) are

$$\begin{pmatrix} \rho \\ \rho U \\ \rho V \\ \rho Z \\ E \end{pmatrix}_t + \begin{pmatrix} \rho U \\ \rho U^2 + p \\ \rho UV \\ \rho ZU \\ (E + p)U \end{pmatrix}_x + \begin{pmatrix} \rho V \\ \rho UV \\ \rho V^2 + p \\ \rho ZV \\ (E + p)V \end{pmatrix}_y = 0$$

where $E = \frac{1}{2}\rho(U^2 + V^2 + (K + 2)/(2\lambda))$ and $p = \rho/(2\lambda)$ is the pressure.

On the other hand, to the first order of τ, the Chapman–Enskog expansion gives $f = g - \tau(g_t + u g_x + v g_y)$ [4]. Taking the moments of ψ to the BGK equation (3) with this f, we get,

$$\int \psi (g_t + u g_x + v g_y) \, \mathrm{d}\Xi = \tau \int \psi (g_{tt} + 2u g_{xt} + u^2 g_{xx} + 2v g_{yt} + 2uv g_{xy} + v^2 g_{yy}) \, \mathrm{d}\Xi$$

from which the compressible Navier–Stokes equations with a dynamic viscous coefficient $\mu = \tau p$, coupled with (2), can be obtained,

$$\begin{pmatrix} \rho \\ \rho U \\ \rho V \\ \rho Z \\ E \end{pmatrix}_t + \begin{pmatrix} \rho U \\ \rho U^2 + p \\ \rho UV \\ \rho ZU \\ (E+p)U \end{pmatrix}_x + \begin{pmatrix} \rho V \\ \rho V \\ \rho V^2 + p \\ \rho ZV \\ (E+p)V \end{pmatrix}_y = \begin{pmatrix} 0 \\ s_{1x} \\ s_{2x} \\ s_{3x} \\ s_{4x} \end{pmatrix}_x + \begin{pmatrix} 0 \\ s_{1y} \\ s_{2y} \\ s_{3y} \\ s_{4y} \end{pmatrix}_y$$

where

$$s_{1x} = \tau p \left[2\frac{\partial U}{\partial x} - \frac{2}{K+2}\frac{\partial U}{\partial x} + \frac{\partial V}{\partial y} \right]$$

$$s_{2x} = \tau p \left[\frac{\partial V}{\partial x} + \frac{\partial V}{\partial y} \right]$$

$$s_{3x} = \tau p \frac{\partial Z}{\partial x}$$

$$s_{4x} = \tau p \left[2U\frac{\partial U}{\partial x} + V\left(\frac{\partial V}{\partial x} + \frac{\partial U}{\partial y} \right) - \frac{2U}{K+2}\left(\frac{\partial U}{\partial x} + \frac{\partial V}{\partial y} \right) + \frac{K+4}{4}\frac{\partial}{\partial x}\left(\frac{1}{\lambda} \right) \right]$$

$$s_{1y} = \tau p \left[2\frac{\partial U}{\partial y} + \frac{\partial V}{\partial x} \right]$$

$$s_{2y} = \tau p \left[\frac{\partial V}{\partial y}\frac{2}{K+2}\left(\frac{\partial U}{\partial x} + \frac{\partial V}{\partial y} \right) \right]$$

$$s_{3y} = \tau p \frac{\partial Z}{\partial y}$$

$$s_{4y} = \tau p \left[U\frac{\partial U}{\partial y} + V\left(\frac{\partial V}{\partial x} + 2V\frac{\partial V}{\partial y} \right) - \frac{2}{K+2}U\left(\frac{\partial U}{\partial x} + \frac{\partial V}{\partial y} \right) + \frac{K+4}{4}\frac{\partial}{\partial y}\left(\frac{1}{\lambda} \right) \right]$$

3. γ-MODEL BGK FLOW SOLVER

In this section, we describe the algorithm formulation for the model derived in the last section by applying the BGK scheme [2–4] and construct the γ-model BGK scheme of second order.

In this paper, only a directional splitting γ-model BGK scheme is presented. The first stage is to reconstruct initial data which are needed in the following dynamical evolution stage. For the second-order scheme, interpolation techniques are used to construct the subcell structure,

here we employ the well-known and useful interpolation technique of limiters, in particular, the Van Leer limiter is used in this paper. Denote by $w_j = (\rho_j, \rho_j U_j, \rho_j V_j, \rho_j Z_j, E_j)$ the cell averaged conservative variables in cell j, by $s_+ = (w_{j+1} - w_j)/\Delta x$ and $s_- = (w_j - w_{j-1})/\Delta x$ their differences between the neighbouring cells. The slope of w in cell j is constructed as,

$$L(s_+, s_-) = s(s_+, s_-)\frac{|s_+||s_-|}{|s_+| + |s_-|}$$

where $s(s_+, s_-) = \text{sign}(s_+) + \text{sign}(s_-)$. After reconstruction, the flow variables are constructed linearly in cell j,

$$\bar{w}_j = w_j + L(s_+, s_-)(x - x_j)$$

The BGK scheme is basically to give a numerical Navier–stokes solution locally under the above initial condition by capturing the time evolution of gas distribution function.

In the evolution stage, we utilize the explicit solution of the BGK model (3) in x direction. The general solution f of (3) at a cell interface $x_{j+1/2}$ and time t is given by

$$f(x_{j+1/2}, t, u, v, z, \xi) = \frac{1}{\tau}\int_0^t g(x', t', u, v, z, \xi)\mathrm{e}^{-(t-t')/\tau}\,\mathrm{d}t' + \mathrm{e}^{-t/\tau} f_0(x_{j+1/2} - ut) \tag{6}$$

where $x' = x_{j+1/2} - u(t - t')$. For the sake of simplicity, $x_{j+1/2} = 0$ will be assumed in the following text. The initial gas distribution function f_0 is assumed to have the form,

$$f_0 = \begin{cases} g^{\mathrm{l}}[1 + a^{\mathrm{l}}x], & x \leqslant 0 \\ g^{\mathrm{r}}[1 + a^{\mathrm{r}}x], & x \geqslant 0 \end{cases} \tag{7}$$

with g^{l}, g^{r} being the Maxwellian distributions at the left and right of a cell interface. Equation (7) means that even with a discontinuity at the cell interface, the gas is assumed to stay in an equilibrium state on both sides of discontinuity, see Reference [50] for more discussions.

The equilibrium state g around $(x = 0, t = 0)$ is assumed to be

$$g = g_0[1 + (1 - H(x))\bar{a}^{\mathrm{l}}x + H(x)\bar{a}^{\mathrm{r}}x] + \bar{A}t \tag{8}$$

where $H(x)$ is the Heaviside function defined by $H(x) = 0$ for $x < 0$ and $H(x) = 1$ for $x \geqslant 0$, g_0 is a local Maxiwillian distribution located at $x = 0$. Notice that g is continuous but has different slopes on both sides of $x = 0$.

In both f_0 and g, $a^{\mathrm{l}}, a^{\mathrm{r}}, \bar{a}^{\mathrm{l}}, \bar{a}^{\mathrm{r}}, \bar{A}$ are related to the derivatives of a Maxwellian in space and time, and assumed to have the following form obtained from a Taylor expansion of a Maxwellian:

$$a^{\mathrm{l}} = a_1^{\mathrm{l}} + a_2^{\mathrm{l}}u + a_3^{\mathrm{l}}v + \tfrac{1}{2}a_4^{\mathrm{l}}(u^2 + v^2 + \xi^2)$$

$$a^{\mathrm{r}} = a_1^{\mathrm{r}} + a_2^{\mathrm{r}}u + a_3^{\mathrm{r}}v + \tfrac{1}{2}a_4^{\mathrm{r}}(u^2 + v^2 + \xi^2)$$

$$\bar{a}^{\mathrm{l}} = \bar{a}_1^{\mathrm{l}} + \bar{a}_2^{\mathrm{l}}u + \bar{a}_3^{\mathrm{l}}v + \tfrac{1}{2}\bar{a}_4^{\mathrm{l}}(u^2 + v^2 + \xi^2)$$

$$\bar{a}^{\mathrm{r}} = \bar{a}_1^{\mathrm{r}} + \bar{a}_2^{\mathrm{r}}u + \bar{a}_3^{\mathrm{r}}v + \tfrac{1}{2}\bar{a}_4^{\mathrm{r}}(u^2 + v^2 + \xi^2)$$

$$\bar{A}^{\mathrm{l}} = \bar{A}_1^{\mathrm{l}} + \bar{A}_2^{\mathrm{l}}u + \bar{A}_3^{\mathrm{l}}v + \tfrac{1}{2}\bar{A}_4^{\mathrm{l}}(u^2 + v^2 + \xi^2)$$

By the reconstruction process described at the beginning of this section, we obtain the distribution $\bar{\rho}_j(x), \bar{\rho}_j\bar{U}_j(x), \bar{\rho}_j\bar{V}_j(x), \bar{\rho}_j\bar{Z}(x), \bar{E}_j(x)$, inside each cell $x_{j-1/2} \leqslant x \leqslant x_{j+1/2}$. Thus, at the cell interface $x_{j+1/2}$, the left and right macroscopic states are

$$\bar{w}_j(x_{j+1/2}) = \begin{pmatrix} \bar{\rho}_j(x_{j+1/2}) \\ \bar{\rho}_j\bar{U}_j(x_{j+1/2}) \\ \bar{\rho}_j\bar{V}_j(x_{j+1/2}) \\ \bar{\rho}_j\bar{Z}_j(x_{j+1/2}) \\ \bar{E}_j(x_{j+1/2}) \end{pmatrix}, \qquad \bar{w}_{j+1}(x_{j+1/2}) = \begin{pmatrix} \bar{\rho}_{j+1}(x_{j+1/2}) \\ \bar{\rho}_{j+1}\bar{U}_{j+1}(x_{j+1/2}) \\ \bar{\rho}_{j+1}\bar{V}_{j+1}(x_{j+1/2}) \\ \bar{\rho}_{j+1}\bar{Z}_{j+1}(x_{j+1/2}) \\ \bar{E}_{j+1}(x_{j+1/2}) \end{pmatrix} \tag{9}$$

from which it follows:

$$\begin{pmatrix} \rho^{\mathrm{l}} \\ U^{\mathrm{l}} \\ V^{\mathrm{l}} \\ Z^{\mathrm{l}} \end{pmatrix} = \begin{pmatrix} \bar{\rho}_j(x_{j+1/2}) \\ \bar{U}_j(x_{j+1/2}) \\ \bar{V}_j(x_{j+1/2}) \\ \bar{Z}_j(x_{j+1/2}) \end{pmatrix}, \qquad \begin{pmatrix} \rho^{\mathrm{r}} \\ U^{\mathrm{r}} \\ V^{\mathrm{r}} \\ Z^{\mathrm{r}} \end{pmatrix} = \begin{pmatrix} \bar{\rho}_{j+1}(x_{j+1/2}) \\ \bar{U}_{j+1}(x_{j+1/2}) \\ \bar{V}_{j+1}(x_{j+1/2}) \\ \bar{Z}_{j+1}(x_{j+1/2}) \end{pmatrix} \tag{10}$$

Using (10) and recalling the definition of a Maxwellian distribution, the left and right Maxwellian distributions g^{l}, g^{r} at $x_{j+1/2}$ are given by

$$\begin{aligned} g^{\mathrm{l}} &= \rho^{\mathrm{l}} \left(\frac{\lambda^{\mathrm{l}}}{\pi}\right)^{(K_j+3)/2} \mathrm{e}^{-\lambda^{\mathrm{l}}[(u-U^{\mathrm{l}})^2+(v-V^{\mathrm{l}})^2+(z-Z^{\mathrm{l}})^2+\xi^2]} \\ g^{\mathrm{r}} &= \rho^{\mathrm{r}} \left(\frac{\lambda^{\mathrm{r}}}{\pi}\right)^{(K_{j+1}+3)/2} \mathrm{e}^{-\lambda^{\mathrm{r}}[(u-U^{\mathrm{r}})^2+(v-V^{\mathrm{r}})^2+(z-Z^{\mathrm{r}})^2+\xi^2]} \end{aligned} \tag{11}$$

where $K_j = 2Z_j - 2$ and

$$\lambda^{\mathrm{l}} = \frac{(K_j+2)\rho_j(x_{j+1/2})}{4(E_j(x_{j+1/2}) - \rho_j(x_{j+1/2})(U_j^2+V_j^2)/2)}$$

$$\lambda^{\mathrm{r}} = \frac{(K_{j+1}+2)\rho_{j+1}(x_{j+1/2})}{4(E_{j+1}(x_{j+1/2}) - \rho_{j+1}(x_{j+1/2})(U_{j+1}^2+V_{j+1}^2)/2)}$$

On the other hand, the relation between the gas distribution function f and the macroscopic variables at $x_{j+1/2}$ gives

$$\int g^{\mathrm{l}}\hat{\psi}\,\mathrm{d}\Xi = \hat{w}_j(x_{j+1/2}); \quad \int g^{\mathrm{l}}a^{\mathrm{l}}\hat{\psi}\,\mathrm{d}\Xi = (\hat{w}_j(x_{j+1/2}) - \hat{w}_j(x_j))/\Delta x^- \tag{12}$$

$$\int g^{\mathrm{r}}\hat{\psi}\,\mathrm{d}\Xi = \hat{w}_{j+1}(x_{j+1/2}); \quad \int g^{\mathrm{r}}a^{\mathrm{r}}\hat{\psi}\,\mathrm{d}\Xi = (\hat{w}_{j+1}(x_{j+1}) - \hat{w}_{j+1}(x_{j+1/2}))/\Delta x^+ \tag{13}$$

where

$$\hat{\psi} = (1, u, v, \tfrac{1}{2}(u^2 + v^2)), \quad \hat{w}_j(x) = (\bar{\rho}_j(x), \bar{\rho}_j \bar{U}_j(x), \bar{\rho}_j \bar{V}_j(x), \bar{E}_j(x))^{\mathrm{T}}$$

$$\Delta x^- = x_{j+1/2} - x_j, \quad \Delta x^+ = x_{j+1} - x_{j+1/2}$$

From (12), the slope a^{l} can be computed from

$$\frac{(\hat{w}_j(x_{j+1/2}) - \hat{w}_j(x_j))}{\rho^{\mathrm{l}} \Delta x^-} = M^{\mathrm{l}}_{\alpha\beta} \begin{pmatrix} a^{\mathrm{l}}_1 \\ a^{\mathrm{l}}_2 \\ a^{\mathrm{l}}_3 \\ a^{\mathrm{l}}_4 \end{pmatrix} \tag{14}$$

where

$$M^{\mathrm{l}}_{\alpha\beta} = \frac{1}{\rho^{\mathrm{l}}} \int g^{\mathrm{l}} \hat{\psi}_\alpha \hat{\psi}_\beta \, \mathrm{d}\Xi = \begin{pmatrix} 1 & U^{\mathrm{l}} & V^{\mathrm{l}} & B_1 \\ U^{\mathrm{l}} & (U^{\mathrm{l}})^2 + 1/(2\lambda^{\mathrm{l}}) & U^{\mathrm{l}} V^{\mathrm{l}} & B_2 \\ V^{\mathrm{l}} & U^{\mathrm{l}} V^{\mathrm{l}} & (V^{\mathrm{l}})^2 + 1/(2\lambda^{\mathrm{l}}) & B_3 \\ B_1 & B_2 & B_3 & B_4 \end{pmatrix}$$

and

$$B_1 = \frac{1}{2} \left\{ (U^{\mathrm{l}})^2 + (V^{\mathrm{l}})^2 + \frac{K_j + 2}{2\lambda^{\mathrm{l}}} \right\}$$

$$B_2 = \frac{1}{2} \left\{ (U^{\mathrm{l}})^3 + (V^{\mathrm{l}})^2 U^{\mathrm{l}} + \frac{(K_j + 4) U^{\mathrm{l}}}{2\lambda^{\mathrm{l}}} \right\}$$

$$B_3 = \frac{1}{2} \left\{ (V^{\mathrm{l}})^3 + (U^{\mathrm{l}})^2 V^{\mathrm{l}} + \frac{(K_j + 4) V^{\mathrm{l}}}{2\lambda^{\mathrm{l}}} \right\}$$

$$B_4 = \frac{1}{2} \left\{ [(U^{\mathrm{l}})^2 + (V^{\mathrm{l}})^2]^2 + \frac{[K_j + 2][(U^{\mathrm{l}})^2 + (V^{\mathrm{l}})^2]}{\lambda^{\mathrm{l}}} + \frac{4K_j^2 + 6K_j + 8}{4(\lambda^{\mathrm{l}})^2} \right\}$$

In the same manner, the coefficient $(a^{\mathrm{r}}_1, a^{\mathrm{r}}_2, a^{\mathrm{r}}_3, a^{\mathrm{r}}_4)$ can be obtained. So, in view of (7), f_0 is determined.

Once f_0 is obtained, the corresponding values of $\rho_0, U_0, V_0, Z_0, \lambda_0$ in

$$g_0 = \rho_0 \left(\frac{\lambda_0}{\pi} \right)^{(K_0+3)/2} \mathrm{e}^{-\lambda_0[(u-U_0)^2 + (v-V_0)^2 + (z-Z_0)^2 + \xi^2]}$$

can be determined as follows, using (6) with $t \to 0$ and the conservation constraint (5) at $(x = x_{j+1/2}, t = 0)$ as well as (7).

$$\int g_0 \psi \, \mathrm{d}\Xi = w_0 = \int_{u>0} \int g^{\mathrm{l}} \psi \, \mathrm{d}\Xi + \int_{u<0} \int g^{\mathrm{r}} \psi \, \mathrm{d}\Xi$$

where $K_0 = (K_j \rho_j + K_{j+1} \rho_{j+1})/(\rho_j + \rho_{j+1})$. Therefore the conservative variables ρ_0, $\rho_0 U_0$, $\rho_0 V_0$, $\rho_0 Z_0$, E_0 at the cell interface can be obtained, and

$$\lambda_0 = \frac{(K_0 + 2)\rho_0}{4E_0 - 2\rho_0(U_0^2 + V_0^2)}$$

from which g_0 is uniquely determined. Then, $\vec{a}^{\mathrm{l}}, \vec{a}^{\mathrm{r}}$ of g can be obtained by the relations,

$$\frac{\hat{w}_{j+1}(x_{j+1}) - \hat{w}_0}{\rho^{\mathrm{l}} \Delta x^-} = \bar{M}^0_{\alpha\beta} \begin{pmatrix} \vec{a}^{\mathrm{l}}_1 \\ \vec{a}^{\mathrm{l}}_2 \\ \vec{a}^{\mathrm{l}}_3 \\ \vec{a}^{\mathrm{l}}_4 \end{pmatrix}$$

and

$$-\frac{\hat{w}_j(x_j) - \hat{w}_0}{\rho^{\mathrm{l}} \Delta x^+} = \bar{M}^0_{\alpha\beta} \begin{pmatrix} \vec{a}^{\mathrm{r}}_1 \\ \vec{a}^{\mathrm{r}}_2 \\ \vec{a}^{\mathrm{r}}_3 \\ \vec{a}^{\mathrm{r}}_4 \end{pmatrix}$$

where

$$\bar{M}^0_{\alpha\beta} = \frac{1}{\rho^{\mathrm{l}}} \int g_0 \hat{\psi}_\alpha \hat{\psi}_\beta \, \mathrm{d}\Xi$$

have the same structure as $M^{\mathrm{l}}_{\alpha\beta}$ only with $\rho^{\mathrm{l}}, U^{\mathrm{l}}, V^{\mathrm{l}}$ and λ^{l} replaced by ρ_0, U_0, V_0 and λ_0.

Up to the point, we have determined all the parameters in the initial gas distribution function f_0 and the equilibrium state g at the beginning of each time step $t = 0$.

Inserting Equations (7) and (8) into (6) and recalling the definition of $H(x)$, we obtain the gas distribution function f at the cell interface,

$$\begin{aligned} f(x_{j+1/2}, t, u, v, \xi) = {} & (1 - \mathrm{e}^{-t/\tau}) g_0 + [\tau(-1 + \mathrm{e}^{-t/\tau}) + t\mathrm{e}^{-t/\tau}] \\ & \times [\vec{a}^{\mathrm{l}} H(u) + \vec{a}^{\mathrm{r}}(1 - H(u))] u g_0 \\ & + \tau \left(\frac{t}{\tau} - 1 + \mathrm{e}^{-t/\tau} \right) \vec{A} g_0 + \mathrm{e}^{-t/\tau}(1 - uta^{\mathrm{l}}) H(u) g^{\mathrm{l}} \\ & + \mathrm{e}^{-t/\tau}(1 - uta^{\mathrm{r}})(1 - H(u)) g^{\mathrm{r}} \end{aligned}$$

where the only unknown left is $\bar{A}$. To determine $\bar{A}$, we integrate the conservation constraint equation (5) at $x_{j+1/2}$ over the whole time step Δt to deduce that

$$\int_0^{\Delta t}\int (g-f)\hat{\psi}\,\mathrm{d}\Xi\,\mathrm{d}t = 0$$

which yields

$$\begin{aligned}\bar{M}^0_{\alpha\beta}\bar{A}_\beta = \frac{1}{\rho_0}\int \{&\gamma_1 g_0 + \gamma_2 u[\bar{a}^{\mathrm{l}}H(u) + \bar{a}^{\mathrm{r}}(1-H(u))]g_0\\ &+\gamma_3[H(u)g^{\mathrm{l}} + (1-H(u))g^{\mathrm{r}}]\\ &+\gamma_4 u[a^{\mathrm{l}}H(u)g^{\mathrm{l}} + a^{\mathrm{r}}(1-H(u))g^{\mathrm{r}}]\}\hat{\psi}_\alpha\,\mathrm{d}\Xi \end{aligned} \tag{15}$$

where

$$\begin{aligned}\gamma_0 &= \Delta t - \tau(1-\mathrm{e}^{-\Delta t/\tau})\\ \gamma_1 &= -(1-\mathrm{e}^{-\Delta t/\tau})/\gamma_0\\ \gamma_2 &= \left(-\Delta t + 2\tau(1-\mathrm{e}^{-\Delta t/\tau}) - \Delta t\mathrm{e}^{-\Delta t/\tau}\right)/\gamma_0\\ \gamma_3 &= (1-\mathrm{e}^{-\Delta t/\tau})/\gamma_0\\ \gamma_4 &= \left(\Delta t\mathrm{e}^{-\Delta t/\tau} - \tau(1-\mathrm{e}^{-\Delta t/\tau})\right)/\gamma_0\end{aligned}$$

Since all moments of the Maxwellian on the right-hand side of (15) can be evaluated, Equation (15) can be uniquely solved.

Finally, the time-dependent numerical flux in the x direction across the cell interface is given by

$$\begin{pmatrix}\mathscr{F}_\rho\\ \mathscr{F}_{\rho u}\\ \mathscr{F}_{\rho v}\\ \mathscr{F}_{\rho z}\\ \mathscr{F}_E\end{pmatrix} = \int u\begin{pmatrix}1\\ u\\ v\\ z\\ \frac{1}{2}(u^2+v^2+\xi^2)\end{pmatrix} f(x_{j+1/2},t,u,v,z,\xi)\,\mathrm{d}\Xi$$

Integrating the above equation to the whole time step, we can obtain the total mass, momentum and energy transport. The above procedure can be repeated in the next time level.

4. NUMERICAL EXAMPLES

In this section we present some numerical examples, which have been tested in the literature by using different schemes, to validate our algorithm for the numerical simulation of inviscid flows. For all the numerical examples in this section, the collision time τ is defined as

$$\tau = \varepsilon \Delta t + \frac{|P_l - P_r|}{P_l + P_r} \Delta t$$

where Δt is the CFL time step, and P_l, P_r are the corresponding pressure in the states g_l, g_r of the initial gas distribution function f_0. With the above collision time the numerical dissipation will be reduced along with the mesh refinement. In the first example we test our scheme in one-space dimension.

Example 1
Sod's Shock problem (see e.g. References [4, 40, 51]).

In this calculation, we take $\varepsilon = 0.54$, the length of the numerical domain is equal to 400 and each cell size is $\Delta x = 1$, the initial condition is

$$W_L = (\rho_L = 1, \rho_L U_L = 0, E_L = 2.5, \gamma_L = 1.4)$$

$$W_R = (\rho_R = 1.25, \rho_R U_R = 0, E_R = 0.5, \gamma_R = 1.2)$$

the initial discontinuity is located at $x = 200$. The simulation results are shown in Figures 1–3 at $t = 60$ for the total density, pressure and γ, respectively. Here we see that the total density, pressure and γ are generally in good agreement with the corresponding numerical results in References [4, 40, 51].

Next, in the following four examples, we test our scheme for two-dimensional problems, and we take all $\varepsilon = 0.5$.

Example 2
Richtmyer–Meshkov instability (see e.g. References [29, 46]).

We consider a shock tube with meshes 480×120, in a two-dimension domain, the initial condition in the tube is composed of an interface separating two fluids of different densities and a shock wave approaching the interface. We take a single mode perturbation of an air–SF_6 interface that the initial location of the interface is represented by

$$x = x_0 - \delta \cos(2\pi y)$$

where $x_0 = 120$ is the location of the unperturbed interface, $\delta = 10$ is the amplitude of the perturbation. We take $\gamma = 1.4, \gamma = 1.093$ for air and SF_6 respectively, and the density ratio $D = \rho_{SF_6}/\rho_{Air} = 5.04$ so as to maintain the constant pressure and temperature across the interface. To trigger the instability, at $x = 110$ there is a planar Mach 1.24 shock wave in air propagating from the left to the right of the interface. Period boundaries on the top and bottom and non-reflecting boundaries on the left and right are considered. It is well-known that this interface becomes unstable after the passage of a shock wave, irrespective of the side

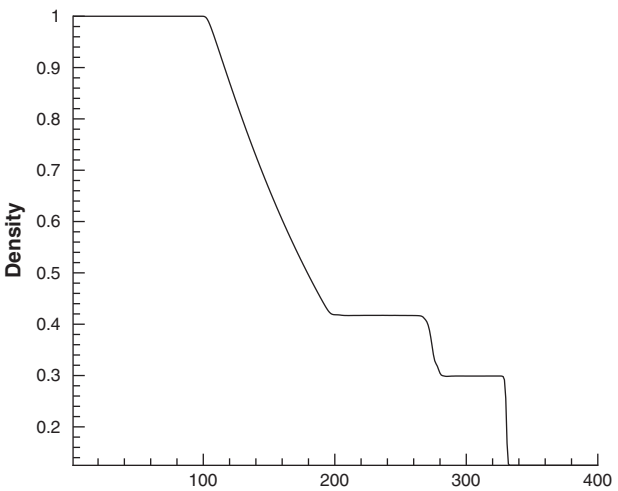

Figure 1. Total density distribution.

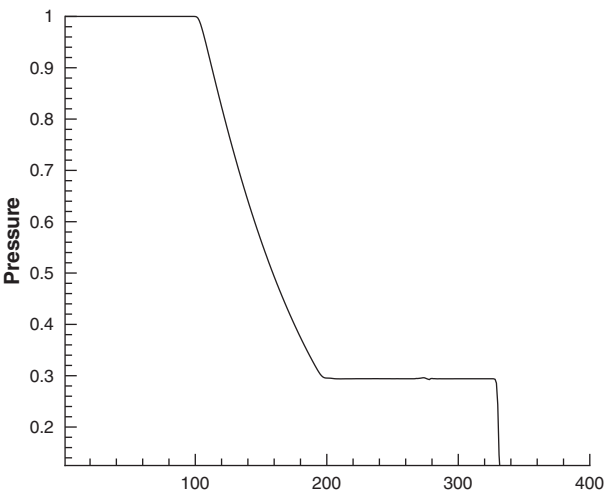

Figure 2. Pressure distribution.

of heavy or light fluid that the shock is incident upon. The numerical results are shown in Figures 4–6 where the contours of the density are given at three different times.

From the figures, the growth of the interface is easily observed. Moreover, it is easy to find that comparing with the same numerical example in References [29, 46], good agreement of the solutions is seen in the large-scale structure.

Example 3

A Mach 1.22 shock hits a R22 cylindrical bubble 1 (see e.g. Reference [23]).

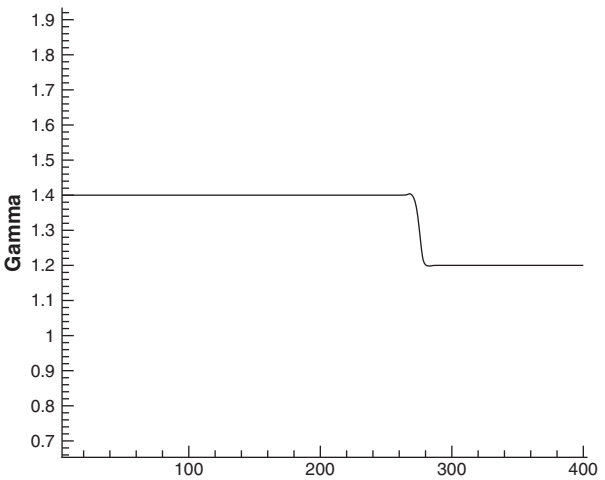

Figure 3. γ distribution.

Figure 4. At time $t = 40$.

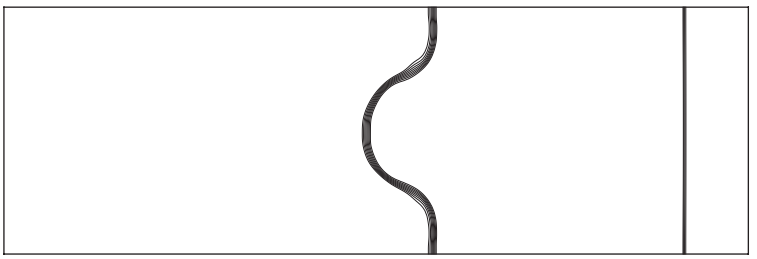

Figure 5. At time $t = 360$.

We examine the interaction of a Mach 1.22 planar shock wave with a cylindrical helium bubble. A schematic description of computational set-up can be found in Reference [42], the initial flow distribution is determined from the standard shock relation with the given strength of the incident shock wave. We use a 480×120 grid, the bubble is assumed to be in both

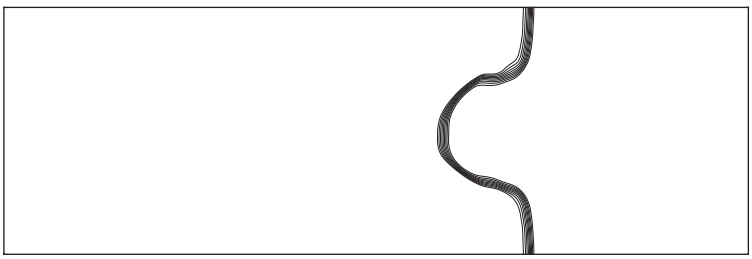

Figure 6. At time $t = 560$. The density distribution of the Richtmyer–Meshkov instability with a Mach 1.24 shock in the air and an air–SF_6 interface.

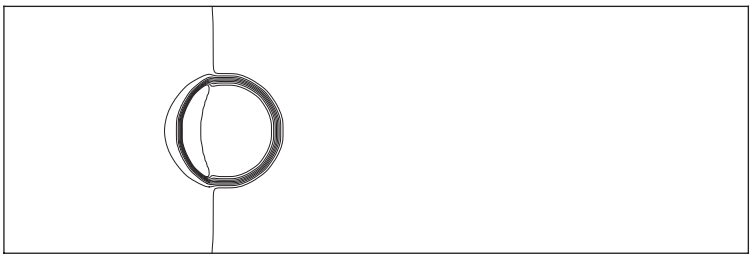

Figure 7. At time $t = 30$.

thermal and mechanical equilibrium with the surrounding air. The non-dimensionalized initial conditions are

$$W = (\rho = 1, U = 0, V = 0, P = 1, \gamma = 1.4), \quad \text{pre-shock air}$$

$$W = (\rho = 1.3764, U = 0.394, V = 0, P = 1.5698, \gamma = 1.4), \quad \text{post-shock air}$$

$$W = (\rho = 3.1538, U = 0, V = 0, P = 1, \gamma = 1.249), \quad \text{R22}$$

reflection boundary conditions on the upper and lower boundaries are used. The results are shown in Figures 7–9 where the contours of the density are given at three different times.

Example 4

A Mach 1.22 shock hits a helium cylindrical bubble (see e.g. References [23, 31, 52]).

We consider the interaction of a Mach 1.22 planar shock wave with a cylindrical helium bubble. We use a 480×120 grid, the bubble is assumed to be in both thermal and mechanical equilibrium with the surrounding air. The non-dimensionalized initial conditions are

$$W = (\rho = 1, U = 0, V = 0, P = 1, \gamma = 1.4), \quad \text{pre-shock air}$$

$$W = (\rho = 1.3764, U = 0.394, V = 0, P = 1.5698, \gamma = 1.4), \quad \text{post-shock air}$$

$$W = (\rho = 0.1358, U = 0, V = 0, P = 1, \gamma = 1.67), \quad \text{helium}$$

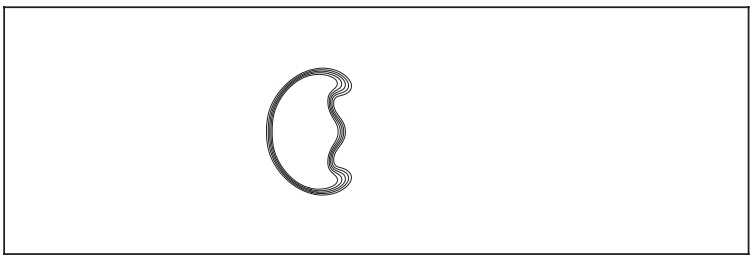

Figure 8. At time $t = 198$.

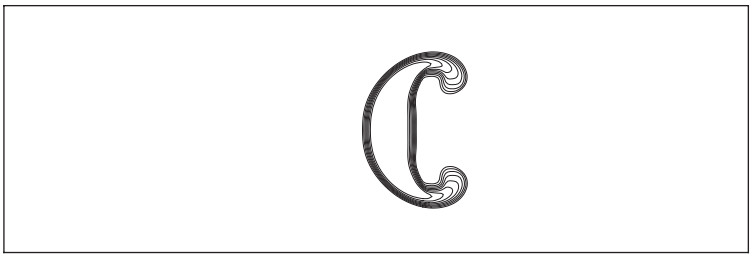

Figure 9. At time $t = 350$. The density distribution of a Mach 1.22 shock hitting a R22 cylindrical bubble.

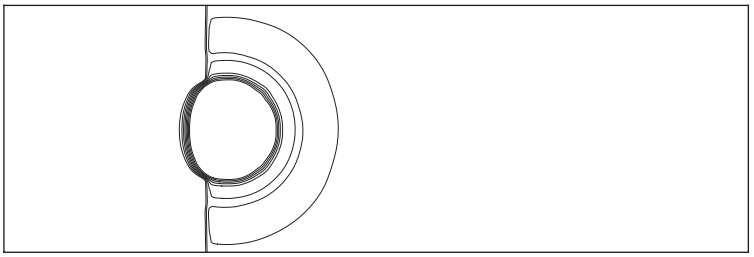

Figure 10. At time $t = 27$.

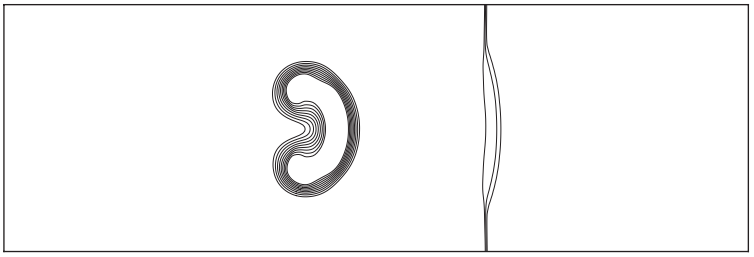

Figure 11. At time $t = 115$.

reflection boundary conditions on the upper and lower boundaries are used. The results are shown in Figures 10–12 where the contours of the density are given at three different times.

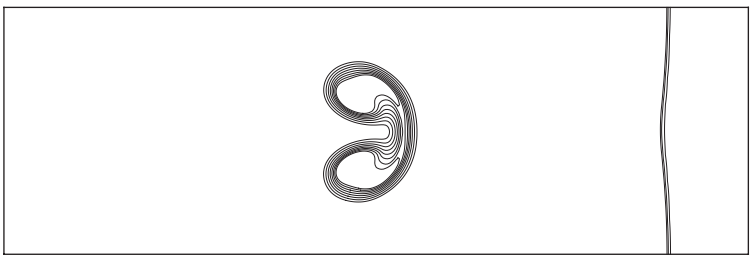

Figure 12. At time $t = 175$. The density distribution of a Mach 1.22 shock hitting a helium cylindrical bubble.

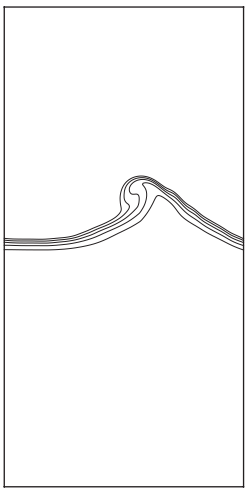

Figure 13. At time $t = 4$.

From Examples 3 and 4, it is easy to see that the simulated results here reproduce the large-scale structure of the corresponding numerical results in References [23, 31, 52] and of the experiments described in Reference [53].

Example 5

Kelvin–Helmholtz instability (see e.g. Reference [29]).

We examine the time evolution for the air–helium case. The gas below the interface is helium. We use a 240×480 grid, and the initial interface is located at

$$y = 320 - 30.0 \cos(2\pi(x - 3)/240)$$

and the non-dimensionalized initial conditions are

$$W = (\rho = 10, U = -25, V = 0.0, E = 25 + 5 \times 25^2, \gamma = 1.4), \quad \text{air}$$

$$W = (\rho = 1.38, U = 25, V = 0.0, E = 10/0.63 + 0.5 \times 1.38 \times 25^2, \gamma = 1.63), \quad \text{helium}$$

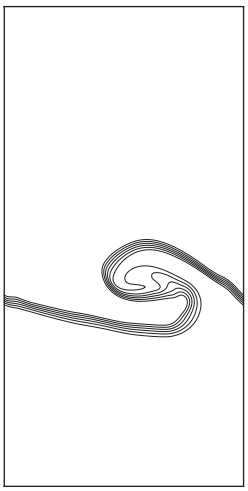

Figure 14. At time $t = 12$.

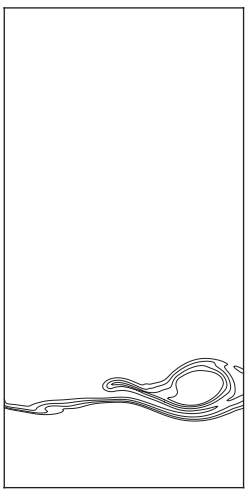

Figure 15. At time $t = 28$. The density distribution of the Kelvin–Helmholtz instability.

The simulated results are shown in Figures 13–15. From the figures, a complex pattern of the interface at later time is observed. Moreover, it is easy to find that comparing with the numerical results given in Reference [54], good agreement of the solutions is seen in the large-scale structure.

5. CONCLUSION

In this paper we present a γ-model BGK scheme for multimaterial flows by incorporating the γ-model scheme in the gas kinetic BGK scheme. Several one- and two-dimensional numerical experiments are carried out, and two-dimensional problem simulations are implemented by applying the directional splitting technique. The numerical results validate the scheme, and the scheme can easily be extended to three space dimensions by applying the technique of directional splitting. A multidimensional γ-model BGK solver, which is defined as a scheme with inclusion of flow gradients in both x and y directions [4], will be studied in a forthcoming paper.

Remark

Recently, a second-order γ-model BGK scheme for multimaterial compressible flows has been proposed by the authors of this paper [A second-order γ-model BGK scheme for multimaterial compressible flows (submitted)]. Numerical examples show that the second-order scheme resolves interfaces better than the first-order one proposed in this paper.

REFERENCES

1. Abgrall R. How to prevent pressure oscillations in multicomponent flow calculation: a quasi conservative approach. *Journal of Computational Physics* 1996; **125**:150–160.
2. Prendergast KH, Xu K. Numerical hydrodynamics from gas kinetic theory. *Journal of Computational Physics* 1993; **109**:53–66.
3. Xu K, Prendergast KH. Numerical Navier–Stokes solutions from gas kinetic theory. *Journal of Computational Physics* 1994; **114**:9–17.
4. Xu K. *Gas Kinetic Scheme for Unsteady Compressible Flow Simulations*, Lecture Note Series 1998-03, Von Kárman Institute for Fluid Dynamics, Rhode St. Genèse, Belgium, 1998.
5. Bhatnagar PL, Gross EP, Krook M. A model for collision processes in gases I: small amplitude processes in charged and neutral one component systems. *Physical Review* 1954; **94**:511–525.
6. Chapman S, Cowling TG. *The Mathematical Theory of Non Uniform Gases*. Cambridge University Press: Cambridge, 1990.
7. Chu CK. Kinetic-theoretic description of the formation of a shock wave. *The Physics of Fluids* 1965; **8**:12–22.
8. Pullin DI. Direct simulation methods for compressible inviscid ideal gas flow. *Journal of Computational Physics* 1980; **34**:231–244.
9. Reitz RD. One-dimensional compressible gas dynamics calculations using the Boltzmann equations. *Journal of Computational Physics* 1981; **42**:108–123.
10. Elizarova TG, Chetverushkin BN. Kinetic algorithms for calculating gas dynamic flows. *Journal of Computational Mathematics and Mathematical Physics* 1985; **25**:1526–1533.
11. Deshpande SM. A second order accurate, kinetic-theory based, method for inviscid compressible flows. *NASA Langley Technical Paper No.* 2613, 1986.
12. Kaniel S. A kinetic model for the compressible flow equations. *Indiana University Mathematics Journal* 1988; **27**:537–563.
13. Croisille JP, Villedieu P. *Kinetic Flux Splitting Schemes for Hyperbolic Flows*, Lecture Notes in Physics, vol. 414. Springer: New York, Heidelberg, 1992.
14. Perthame B. Second-order Boltzmann schemes for compressible Euler equations in one and two space dimensions. *SIAM Journal on Numerical Analysis* 1992; **29**:1–19.
15. Mandal JC, Dasphande SM. Kinetic flux vector splitting for Euler equations. *Computers and Fluids* 1994; **23**:447–478.
16. Croisille JP, Khanfir R, Chanteur G. Numerical simulation of the MHD equations by a kinetic type method. *Journal of Scientific Computing* 1995; **10**:81–92.
17. Chou SY, Baganoff D. Kinetic flux-vector splitting for the Navier–Stokes equations. *Journal of Computational Physics* 1997; **130**:217–230.
18. Wu H, Tang H. Computation of multicomponent flows of Euler equations. *LCP Annual Report 1998*, IAPCM, Beijing, 1998; 208–213 (Chinese).
19. Xu K, Martinelli L, Jameson A. Gas-kinetic finite volume methods, flux-vector splitting and artificial diffusion. *Journal of Computational Physics* 1995; **120**:48–65.

20. Xu K, Kim C, Martinelli L, Jameson A. BGK-based schemes for the simulation of compressible flow. *International Journal of Computational Fluid Dynamics* 1996; **7**:213–235.
21. Kim C, Xu K, Martinelli L, Jameson A. Analysis and implementation of the gas-kinetic BGK scheme for computational gas dynamics. *International Journal for Numerical Methods in Fluids* 1997; **25**:21–49.
22. Xu K. BGK based scheme for multicomponent flow calculations. *Journal of Computational Physics* 1997; **134**:122–133.
23. Lian YS, Xu X. Gas-kinetic scheme for multimaterial flows and its application in chemical reactions. *Journal of Computational Physics* 2000; **163**:349–375.
24. Xu K. Gas kinetic theory based flux splitting method for ideal magnetohydrodynamics. *Journal of Computational Physics* 1999; **153**:334–352.
25. Tang HZ, Xu K. A high-order gas-kinetic method for multidimensional ideal magnetohydrodynamics. *Journal of Computational Physics* 2000; **165**:69–88.
26. Kim C, Jameson A. A robust and accurate LED-BGK solver on unstructured adaptive meshes. *Journal of Computational Physics* 1998; **143**:598–627.
27. Xu K. Discontinuous Galerkin BGK (DG-BGK) method for viscous flow equations: one-dimensional systems, 2002, preprint.
28. Osher S, Sethian JA. Fronts propagating with currature-dependent speed: algorithms based on Hamilton-Jacobi formulations. *Journal of Computational Physics* 1988; **79**:12–49.
29. Mulder M, Osher S, Sethian JA. Computing interface motion in compressible gas dynamics. *Journal of Computational Physics* 1992; **100**:209–228.
30. Peng D, Merriman B, Osher S, Zhao H, Kang M. A PDE-based fast local level set method. *Journal of Computational Physics* 1999; **155**:410–438.
31. Fedkiw RP, Aslam T, Merriman B, Osher S. A non-oscillatory Eulerian approach to interfaces in multi material flows (the Ghost Fluid method). *Journal of Computational Physics* 1999; **152**:457–492.
32. Sethian JA. *Level Set Methods and Fast Marching Methods*. Cambridge University Press: Cambridge, 1999.
33. Osher S, Fedkiw RP. Level set methods: an overview and some recent results. *Journal of Computational Physics* 2001; **169**:463–502.
34. LeVeque RJ. Wave propagation algorithms for multidimensional hyperbolic system. *Journal of Computational Physics* 1997; **131**:327–353.
35. Wang SP, Anderson MH, Oakley JG, Coradini ML, Bonazza R. A thermodynamically consistent and fully conservative treatment of contact discontinuities for compressible multicomponent flows. *Journal of Computational Physics* 2004; **195**:528–559.
36. Saurel R, Abgrall R. A simple method for compressible multifluid flows. *SIAM Journal on Scientific Computing* 1999; **21**:1115–1145.
37. Noh WF, Woodward P. SLIC (simple line interface calculation). *Proceedings of the 5th International Conference on Numerical Methods in Fluid Dynamics*. Lecture Notes in Physics, vol. 59. Springer: New York, Heidelberg, 1976; 330–340.
38. Youngs DL. In *Time-dependent Multi-material Fluid Dynamics*, Morton KW, Baines MJ (eds). Academic Press: New York, 1982; 273–285.
39. Roe PL. A new approach to computing discontinuous flow of several ideal gases. *Technical Report*, Cranfield Institute of Technology, 1984.
40. Karni S. Multicomponent flow calculations by a consistent primitive algorithm. *Journal of Computational Physics* 1994; **112**:31–43.
41. Algrall R, Karni S. Computations of compressible multifluids. *Journal of Computational Physics* 2001; **169**(169):594–623.
42. Karni S. Hybrid multifluid algorithms. *SIAM Journal on Scientific Computing* 1997; **17**:1019–1039.
43. Ton V. Improved shock-capturing methods for multicomponent and reacting flows. *Journal of Computational Physics* 1996; **128**:237–253.
44. Jenny P, Mueller B, Thomann H. Correction of conservative Euler solvers for gas mixtures. *Journal of Computational Physics* 1997; **132**:91–107.
45. Toro EF. Primitive, conservative and adaptive schemes for hyperbolic conservation laws. In *Numerical Methods for Wave Propagation (Manchester 95)*, Toro EF, Clarke JF (eds). Kluwer Academic Publishers: Dordrecht, 1998; 253–274.
46. Shyue KM. An efficient shock capturing algorithm for compressible multicomponent problems. *Journal of Computational Physics* 1998; **142**:208–242.
47. Saurel R, Abgrall R. A multiphase Godunov method for compressible multifluid and multiphase flows. *Journal of Computational Physics* 1999; **150**:425–467.
48. Shyue KM. A fluid-mixture type algorithm for compressible multicomponent flow with Van der Waals equation of state. *Journal of Computational Physics* 1999; **156**:43–88.
49. Lian YS, Xu K. A gas-kinetic scheme for reactive gas. HKUST, HongKong, 2002, preprint.
50. Xu K. A gas-kinetic BGK scheme for the Navier–Stokes equations and its connection with artificial dissipation and Godunov method. *Journal of Computational Physics* 2001; **171**:289–335.

51. Larrouturou B. How to preserve the mass fraction positive when computing compressible multi-component flow. *Journal of Computational Physics* 1991; **95**:59–84.
52. Quirk JJ, Karni S. On the dynamics of a shock bubble interaction *Journal of Fluid Mechanics* 1996; **318**: 129–163.
53. Haas JF, Sturtevant B. Interactions of weak shock waves with cylindrical and spherical gas inhomogeneites. *Journal of Fluid Mechanics* 1987; **181**:41–76.
54. Fedkiw RP, Liu XD, Osher S. A general technique for elimination of spurious oscillations in conservative scheme for multi phase and multi species Euler equations. *UCLA CAM Report* 97-27, 1997.
55. Colella P, Majda A, Roytburd V. Theoretical and numerical structure for reacting shock waves. *SIAM Journal on Scientific and Statistical Computing* 1986; **7**:1059–1080.

